Lab on a Chip

Accepted Manuscript

ROYAL SOCIETY OF CHEMISTRY

www.rsc.org/loc

Cite this: DOI: 10.1039/c0xx00000x

www.rsc.org/xxxxxx

ARTICLE TYPE

Strong vortical flows generated by the collective motion of magnetic particle chains rotating in a fluid cell

Yang Gao,[a,b] Jasper Beerens,[a] Alexander van Reenen,[b,c] Martien A. Hulsen,[a] Arthur M. de Jong,[b,c] Menno W.J. Prins,[b,c] and Jaap M.J. den Toonder*[a,b]

Received (in XXX, XXX) Xth XXXXXXXXX 20XX, Accepted Xth XXXXXXXXX 20XX

DOI: 10.1039/b000000x

Magnetic microparticles, assembled into chains that are actuated with rotating magnetic fields, can be used as microstirrers to promote fluid transport and biochemical reactions in microfluidic systems. We show that, within a certain range of magnetic field rotation frequency, the microstirrers exhibit a coherent collective motion: the rotating magnetic particle chains move throughout the volume of a flat fluid cell and generate very strong (~1 mm/s) and global (9 mm) vortical fluid flows, with many eddy-type substructures that fluctuate continuously in time, resembling turbulent flow. The collective motion makes the microstirrers not only defy gravity, but also to move against magnetic field gradients. The induced fluid flow is directly related to the stirring rate and the amount of magnetic particle chains. The observed behavior is caused by the magnetic and hydrodynamic interactions between the magnetic microparticles and the fluid. We utilized the phenomenon of swarming particles to enhance biochemical assays with magnetic capture particles (4000/μL) and IgG targets (500 pM). When compared to a reference system of sedimented magnetic capture particles, magnetic actuation leads to both a ~9 times increase in the initial assay kinetics as well as a ~7 times increase of target capture signal after 30 minutes.

Introduction

Magnetic microparticles have many applications in microscale systems, for example as actuators[1,2,3] to generate fluid flows, as stirrer[4,5,6,7,8] to mix laminar fluid streams and when functionalized with bio-specific surface coatings, as mobile binding-sites for biochemical assays[9,10,11,12,13]. Critical reviews of magnetic particles in microfluidic systems are presented by Pamme[14] and Gijs[15]. The rapid response of the particles to applied magnetic fields and the induced formation of structures such as chains and columns make the utilization of magnetic particles as microactuators in microscale systems attractive for both research and industry.

One of the most well-known strategies for microscale mixing is the stirrer-strategy, i.e. a suspension of magnetic particles is exposed to a uniform biaxial rotating magnetic field, thereby creating rotating chains of magnetic particles that act as programmable microstirrers[4,5,6]. Within a specific range of magnetic field magnitude, rotational frequency and fluid and particle properties, chains of magnetic particles periodically break-up and self-assemble, thereby inducing chaotic mixing of the fluid and enhanced particle-based target capture in biochemical assays[16,17,18]. Simultaneous with the rotational dynamics of the magnetic particle chains, additional field gradients can be applied, perpendicular to the rotating field, to translate the rotating particle chains, so that they can interact with the whole sample volume.

In this paper, we present a novel method to generate strong fluid flows utilizing rotating particle chains of low magnetic content in a flat fluid cell. Interestingly, we found that above a certain rotational frequency of the applied field, the local stirring of fluid by the particle chains becomes coupled with the global induced fluid flow, and thereby creates clouds of particles moving throughout the mm-sized volume of the fluid cell. A movie (Video S1) depicting the observed phenomenon is available in the Electronic Supplementary Information. When viewed more closely, the cloud of particles appears to consist of small particle chains and clusters whirling like dervishes without creating static clusters or aggregates. Eventually, this initial and chaotic motion of swarming particles transits into a steady-state regime with magnetic microstirrers translating in opposite directions along the upper and bottom layers of the fluid cell, i.e. a continuous vortex flow of fluid and particles is established. We visualized and characterized the induced vortical flows of fluid and particles, containing many eddy-type substructures that fluctuate continuously in time, and for which the direction and flow characteristics can be directly controlled by the external magnetic field. We also report the effectiveness of strong vortical flows to perform microscale mixing and microscale biochemical assays.

Materials and methods

Magnetic actuation setup

[Figure 1 here]

We used a home-built magnetic actuation setup to create well controlled time-dependent magnetic fields within a microfluidic device placed at its centre, see Fig. 1(a)[19]. The setup consists of eight individually controlled copper coils together with 8 soft-iron poles connected by soft-iron frames. Magnetic fields are produced by the flow of electrical currents through the coils and by following the soft iron frames, they are guided to the center of the setup where a closed fluid cell is placed containing a suspension of (magnetic) particles. In the experiments we report in this paper, we use four vertical and, and four horizontal poles for the generation of the vertical (z-y) and horizontal (x-y) components of the magnetic fields, respectively. The soft iron poles have a square cross section of 5 mm by 5 mm, and are spaced 14 mm from each other. Horizontally or vertically rotating fields are obtained by applying sinusoidal signals to the individual poles belonging to either the horizontal or the vertical poles, with a phase lag of 90° between consecutive poles. In some experiments, a combined horizontally and vertically rotating field is applied. The magnitude of the applied field is 30 mT or 5 mT; the rotation frequencies are between 5 and 300 Hz. The fluid cell is a flat cylindrical chamber with a diameter of 9 mm and height of 600 µm, and it is closed with glass substrates.

In the experiments presented in this paper, the details of the applied magnetic fields are important. Therefore, we present calculations of the generated fields as a function of the electromagnetic driving schemes. The simulation of the generated magnetic field was conducted under the assumption of magnetostatics, which holds for magnetic fields in systems where the currents are steady (i.e. not changing rapidly with time). The governing equations are (1) Gauss's law for magnetism, $\vec{\nabla} \cdot \vec{B} = 0$, (2) Ampère's law, $\vec{\nabla} \times \vec{H} = \vec{J}$, (3) time invariance, $\partial \vec{B} / \partial t$, (4) $\vec{B} = \mu_0 \mu_r \vec{H}$. In these equations, $\vec{B}$ is the magnetic induction (often referred to as 'magnetic field'), $\vec{H}$ is the magnetic field, $\vec{J}$ is the (steady) current, μ_r is the relative permeability and μ_0 is the permeability of free space. The results were obtained by modeling the setup in a 3D commercial FEM package (Comsol Multiphysics®). The soft-iron and copper materials were modeled as linear media with relative permeabilities (μ_r) of 4750 and 1, respectively. The number of degrees of freedom used to simulate the setup was 7133192.

In Fig. 1(b), the magnetic particles at the cell floor are exposed to a rotating vertical magnetic field that is created by applying sinusoidal signals to the four vertical magnetic poles (highlighted in red in the figure), with a 90° phase lag between the signals. On the right side of the figure, the time-averaged magnitude of the magnetic field over one rotational cycle is plotted over the entire cell region (9 mm x 9 mm) at z=0, i.e. the fluid cell floor. Due to the geometry of the setup and, in particular, the orientation of the vertical poles (red) with respect to the fluid cell, a narrow band region (between x=-2 mm and x=2 mm) with high field strengths is formed. Since the magnetic particles move up the field gradient, i.e. the particles move towards regions of highest field strengths, this `band region' will cause the magnetic particles to be confined along the entire length of the fluid cell without any dispersion.

The influence of a triaxial magnetic field is investigated by superimposing a rotating vertical magnetic field on a rotating horizontal magnetic field. In Fig. 1(c), the applied magnetic fields have equal magnitudes and equal frequencies. As expected, the rotational plane experienced by the particle chains is between the vertical and the horizontal planes. However, when studying the corresponding time-average field magnitudes, we observe that the critical `band region' is broken down into isolated islands, located near the horizontal poles. This is caused by the adjacent geometrical positions of the horizontal poles with respect to the horizontally placed fluid cell. In order to retain the critical band region, a triaxial magnetic field is constructed in Fig. 1(d) with a dominating vertical magnetic field (4 times larger in magnitude than the horizontal field). Indeed, the band region of high field strength is restored but less confined due to the influence of the horizontal poles.

These calculation results show, that the electromagnetic driving scheme determines the details of the magnetic field distribution within the fluid cell, and therefore determines the motion of the magnetic microparticles suspended in the fluid cell.

Materials

The magnetic particles used in the experiments are 10 µm super-paramagnetic Micromer® -M particles (~4000/µL) with a mass density that is similar to water ($1.1 \bullet 10^3$ kg/m^3). These particles were dispersed in water. The magnetic susceptibility of the particles is $\chi_p \sim 0.1$ (according to information from the manufacturer). To visualize the induced fluid flow, we used as tracer particles 2 µm FluoSpheres® (~2000/µL). Both the magnetic and the fluorescent particles are coated with carboxylic-acid groups to ensure stable particles in aqueous media. For biochemical assay experiments, we coated the magnetic particles with (Recombinant) Protein G (Calbiochem®) proteins to create magnetic capture particles. The assay targets are Goat anti-Mouse IgG with Alexa dye 488 fluorescent labels. The assay components are suspended in a buffer solution (PBS + 1 mg/ml BSA) before introducing into the fluid cell.

In our experiments, we minimize the particle-surface interactions by using magnetic particles with low magnetic content, i.e. with a mass density that is similar to water, which minimizes the influence of gravity. Moreover, both the glass surfaces of the fluid cell[20] and the carboxylated magnetic particles we use are known to acquire negative surface charges when immersed in water, giving low surface interactions. This means that our experimental conditions are very different from the work of Sing et al.[1], who observed individual chains of particles walking over a surface in a rotating field, caused by strong gravitational interactions with the surface.

Biochemical assay protocol

For the biochemical assay, we used magnetic particles (4000/µL) coated with Protein G proteins to capture the uniformly distributed IgG assay targets (500 pM) within a flat fluid cell.

Utilizing the octopolar setup, a single rotating vertical magnetic field or a combination of two fields is used to generate strong and chaotic vortical flows of fluid and particles. As a reference, we performed experiments where the magnetic particles were allowed to remain sedimented at the bottom cell floor with no external actuation (passive measurements). The capture of the targets onto the magnetic particles was measured by acquiring the emitted fluorescent intensities from the magnetic particles utilizing fluorescence microscopy (Leica® DM-4000 microscope with Andor® Luca camera). Also we obtain the emitted fluorescent intensities of the background, i.e. the fluid. The difference between the two data sets gives an accurate indication of the amount of captured targets onto the magnetic particles. See the Electronic Supplementary Information for more details.

Results and discussion

Collective particle motion

[Fig. 2 here]

Fig. 2 shows images of the suspended magnetic microparticles within the fluid cell, at different locations in the cell and as a function of different actuation protocols. The particles are initially sedimented on the fluid cell floor. Without magnetic actuation (a) the magnetic particles are located at the center of the fluid cell. A clockwise rotating vertical magnetic field (B, 30 mT, 1 Hz) is applied and the magnetic particles form chains that follow the applied field (movies of the experiments (Video S2) are available in the Electronic Supplementary Information). Besides the generated magnetic field, the magnetic setup also induces a band region of high field strengths with local maxima occurring near the (red) vertical poles and at the center of the fluid cell (Fig. 1(b)). The generated field gradients have severe consequences for the motion of the microparticles since they effectively confine the rotating particle chains near the center of the fluid cell (b) and trap and aggregate the particles at the poles (c), effectively terminating the rotational and translational movements of the microstirrers.

However, when the rotational frequency of the applied field is increased to 30 Hz, we observe a different phenomenon. A strong and chaotic vortical flow of a ‘cloud’ of particles (Fig. 2(d), Video S1) is released. The cloud of particles consists of small particle chains and clusters whirling vigorously. More importantly, the collective motion of the particles transits to a steady state phenomenon, i.e. eventually a stable and continuous clockwise vortex flow of individually rotating chains is formed along the entire length of the fluid cell, seemingly defying both gravity and magnetic field gradients (Video S3). The time-dependent formation of such global vortex flow is described in the Electronic Supplementary Information, section “Time-dependent formation of swarming”. Indeed, if we reverse the applied field, i.e. a counter-clockwise rotating magnetic field is applied, we observe the inversed translational movement of the swarm.

The emergence of coordinated collective motion we observe here resembles swarming behavior. This has been observed in many biological and man-made systems, from bacterial swarms to animal flocks to colloidal systems[21]. It has been proposed that this collective behavior can in principle be solely accounted for by a limited set of alignment rules at the local, individual level[22,23,24,25]. However, more intricate systems have been observed in which local alignment rules are entangled with more complex, and often unknown, larger scale interactions [21].

In our case, the observed phenomena can be explained qualitatively by a combination of local and global interactions. (I) On a local level, the magnetic interactions between the particles cause the particles to form dynamic particle chains that rotate within the fluid. The details of the chain dynamics are also influenced by the viscous drag that the chains experience, and at the same time the chains act as microstirrers that generate local fluctuating vertical flow. (II) On a global level, in a geometrically confined fluid volume like our fluid cell, the stirring of the fluid by the rotating chains, added up collectively, will induce a global vortex flow of fluid and particles in the same rotational direction. (III) However, this vortex flow is initially hindered by magnetic gradient forces that trap and concentrate the particles at the opposite ends of the fluid cell (i.e. Fig. 2(c). (IV) At a critical rotational frequency of 30 Hz, the superposition of local stirring of the fluid by the individual microstirrers induces such a strong global fluid flow that the magnetic gradient forces are overcome, i.e. the ``trapped'' magnetic particle chains move with the flow and a strong and chaotic (back)flow of a cloud of particles is released (i.e. Fig. 2(d)). The system is then in the regime where the local stirring of the fluid, caused by the applied fields, is coupled with the more globally induced vortex flow, influenced by the geometrical dimensions of the fluid cell. More importantly, in this regime, the magnetic microstirrers both generate and move with the fluid flow.

The different regimes of the collective particle behavior

[Fig. 3 here]

In Fig. 2, the rotational frequency for the magnetic particle chains to overcome the gradient forces and to spread out over the fluid cell length is found to be at 30 Hz at limited field strength of 30 mT. At lower stirring rates (Fig. 3, Video S4) of the microstirrers, we observe a significant loss of magnetic particles to the opposite ends of the fluid cell and the formed cloud of microstirrers diminishes over time. We attribute this to the strong field gradients present near the vertical poles, attracting and trapping the magnetic particles to form stationary clusters and aggregates. The system is in a regime (5 Hz and 10 Hz) where the dynamics of the magnetic particles are predominantly determined by forces due to magnetic field gradients (∇B^2).

A shown in Fig. 3, at higher rotational frequency (30 and 50 Hz) of the applied field, the magnetic gradient forces are overcome and a stable and well-defined vortex flow of rotating particle chains is established. In this regime, the local fluid stirring generated by individual microstirrers adds up to create a global vortex flow of fluid and particles.

At even higher rotational frequency (70 and 90 Hz) of the applied field, the flow of microstirrers becomes confined at one end of the fluid cell. This is due to the dominant viscous drag acting on the individual rotating magnetic particle chains, preventing them

to follow the applied field. Generally, rotating magnetic particle chain dynamics are characterized by the use of the Mason number[1,26], defined as the ratio of viscous to magnetic forces, i.e. $M_n \sim \eta f / B^2$ with η the viscosity of the fluid, f the rotating field frequency and B the magnitude of the applied field. Here, η is 1 mPa•s, B is kept constant at 30 mT and the rotational frequency of the applied field is varied. At low Mason numbers (f=1 Hz), magnetic particles aggregate into long vertical chains that follow the applied field. At higher Mason numbers (f=30 Hz), the viscous forces prevent the magnetic particles to form long particle chains and instead, smaller chains and clusters appear. We performed high speed camera measurements to monitor the rotational dynamics of the rotating chains and they indeed follow the applied field at a field rotation rate of 30 Hz. However, when the field rotational frequency is increased up to 50 Hz to achieve even higher Mason numbers, the chains cannot keep up with the field anymore and they rotate with a delayed stirring rate of 15 Hz.

It is also interesting to explore the possibility of creating the collective particle behavior when exposing the magnetic particle suspension to a triaxial magnetic field, i.e. the combination of a horizontal rotating magnetic field with a vertical rotating magnetic field. As we show in the Electronic Supplementary Information: "Triaxial Control", the influence of the additional horizontal fields results in a stable but stretched, i.e. spread out, vortex flow of magnetic colloidal particles.

The induced fluid flow

[Fig. 4 here]

We experimentally visualized and characterized the local and global induced fluid flow generated by the motion of the rotating magnetic particle chains. We anticipated that the collective particle motion would produce significant microfluidic flows, which will be important in achieving fast mixing and/or fast biochemical reactions in microfluidic systems.

At the left-side of Fig. 4, a vertical counter-clockwise rotating magnetic field (30 mT, 30 Hz) is applied and we monitor the induced fluid flow by capturing the motions of fluorescent tracer particles added to the fluid (2 μm, white spots), as indicated by the red arrows, in different horizontal planes over the entire height of the fluid cell. As Fig. 4 shows, a global counter-clockwise rotating vortex fluid flow is established, with tracer particles at the bottom (z=0 μm) and upper (z=600 μm) surfaces moving unidirectionally (right-side of Fig. 4), i.e. moving to the right and the left, respectively. At the center of the fluid cell (z=300 μm), the unidirectional motion disappears, and small, local and short-living vortices appear. Ideally, in a system in which the magnetic particles are equally distributed among the upper and bottom layers of the fluid cell, the net shear forces/fluid flows at the center plane equal zero. However, in our experiments, the magnetic particles are not equally distributed among the different planes of the fluid cell and more importantly, the individually rotating chains themselves are also subjected to the induced fluid flow, resulting in the formation of local vortices/perturbations at the center of the cell.

[Fig. 5 here]

To keep the particles distributed over the entire length of the fluid cell, the induced fluid flow should be strong enough to overcome the magnetic gradient forces trapping the magnetic particles near the poles. More specifically, in this regime, the magnetic particle chains both generate and move with the global induced fluid flow. In Fig. 5a, we show the magnitudes of translational velocities of both the tracer particles and the magnetic particle chains at a stirring rate of 30 Hz (vertical field) in different horizontal planes of the fluid cell. Near the surfaces of the fluid cell, a strong fluid flow with a magnitude of ~0.9 mm/s is observed. At the center of the fluid cell and due to the vortex structure of the flow, the flow magnitude decreases to ~0.1 mm/s. Similar velocities are also observed for the magnetic microstirrers which indeed confirms our assumption that in this regime, the microstirrers move with the global induced fluid flow, and thereby overcome magnetic gradient forces. To investigate the influence of inertial effects in generating the global induced fluid flow, we turned the rotating vertical magnetic field (30 mT, 30 Hz) suddenly on and off (Video S6). Accordingly, we observed instantaneous start or stand-still of the motion of the tracer particles. Although the Reynolds number, i.e. $Re = \rho v L / \eta$ with ρ the density of water, v the flow velocity (~0.9 mm/s), L the length scale of the system (~9 mm) and η the viscosity of water, is above one, namely about 10, the influence of inertia still seems negligible. The Reynolds number based on the microparticles is orders of magnitude smaller, i.e. it is much smaller than one. For sure, although we observe very chaotic fluid behavior, this observation also proves that the flow is not turbulent.

We also measured (Fig. 5b) the induced fluid flow at a lower stirring rate (15 Hz). Since the net fluid flow at the center is predominantly caused by the inhomogeneous distribution of the magnetic particles within the fluid cell, the fluid flows near the surfaces are believed to represent the most reliable relationship between local stirring of fluid and the global induced vortex flow. Indeed, we expect and measured a two-fold lower fluid velocity at a two-fold lower stirring rate of the micro-stirrers, i.e. ~0.9 mm/s for 30 Hz and ~0.45 mm/s for 15 Hz. Moreover, in Fig. 5c we compare the differences in the induced flow between the initial and the final (vortex) stage of actuation. In the initial stage, all the magnetic particles are present at the bottom surface of the fluid cell whereas in the final stage, their presence is equally distributed between the upper and bottom surfaces of the fluid cell. In accordance with the distribution of the particles, we see at the bottom surface of the fluid cell and in the initial stage, a flow velocity of ~1.9 mm/s which is about twice the magnitude of the flow velocity (~0.9 mm/s) in the final stage. This shows that the distribution of the microstirrers over the fluid volume is an important determining factor for the global flow morphology

As indicated above, a triaxial magnetic field causes the motion of the particle chains to be spread out over a volume, which can be beneficial for enhanced mixing or homogenization processes. It is interesting to see whether the rotating particle chains, with their dynamic behavior now controlled by a combination of a horizontal (5 mT, 300Hz) and a vertical (30 mT, 30 Hz) magnetic field, can still generate strong global microfluidic flows. In Fig. 5d, it is shown that the triaxial motion of the micro-stirrers indeed still generates strong fluid flows (~0.8 mm/s).

Mixing and Biochemical assay experiments

As a next step, we investigated the possibility of using the phenomenon of collective particle motion to achieve fast mixing and/or homogenization of fluids within the fluid cell. A qualitative analysis was carried out by seeding the fluid with fluorescent tracer particles (2 μm) and waiting for 2 hours for the tracer particles to sediment onto the bottom surface of the fluid cell. Next, we turned on the vertical rotating magnetic field (30 mT, 30 Hz) and monitored the distribution of the fluorescent tracer particles along the entire height of the fluid cell. Indeed, we observed total re-suspension of fluorescent tracer-particles after 1 min of actuation which indicates that the phenomenon of `swarming particles' can be used to achieve fast homogenization of fluids in microscale systems (Video S7).

[Fig. 6 here]

Finally, we report the effectiveness of utilizing these strong vortical flows to perform microscale biochemical assays with magnetic capture particles (~4000 μL) and IgG targets (500 pM) marked with fluorescent dyes (Fig. 6). The amount of captured targets is quantified by the net fluorescence intensity emitted from the magnetic capture particles, i.e. the difference between the emitted fluorescence intensities from the magnetic capture particles and the background fluid. Initially (first measurement points), the net fluorescence intensity is found to be negative: no targets are bound onto the particles and the background fluid (seeded with the targets) emits higher fluorescence. As the targets are captured from the fluid and onto the magnetic capture particles, the emitted fluorescence of the background fluid drops in intensity.

In the case of passive/reference measurements (no external fields), the signal (diamonds in Fig. 6) slowly approaches a value around 100 due to the depletion of the targets in the vicinity of the sedimented magnetic capture particles. Also, the initial assay kinetics are slowed down by the limited diffusive mass-transport of the targets towards the magnetic capture particles: with a maximum diffusion distance equal to the length scale of the system (i.e. the width of the fluid cell which is 9 mm). To compare, AFM studies of non-labeled IgG showed that a single non-labeled IgG molecule is 20-40 nm in diameter[27]. The root-mean-square displacement of a (spherical) target particle with a diameter of 20 nm after 100 minutes is about 0.5 mm. Taken into account the relatively large length scale of the system, only a small amount of the targets are captured from the sample volume after 30 minutes. This leads to the differences in the ``saturation'' levels between the passive and the active target capture signals.

In case of magnetic actuation and due to the formed vortical flow of magnetic particle chains, the magnetic particles translate across the entire length (9 mm) of the fluid cell periodically and in a relatively short amount of time (~10 s), which will certainly decrease the limiting diffusion distance of the targets and increase the initial assay kinetics. Also the strong vortical flows of fluid and particles constantly refresh the surroundings of the magnetic particle chains, which will diminish the occurrence of any target depletion and, consequently saturation of the signal. We should note that, even thought the triaxial actuation protocol leads to more spreading of the magnetic capture particles (as shown in Fig. S2 of the ESI), it does not result in a significantly faster target capture than the biaxial rotation scheme. It seems that the constant reduction of depletion in combination with the overall strong vortical flow is the dominant enhancing factor in our experiments. Overall, when compared with passive measurements, we observe that (1) the initial slope of the signals (circle and square) leads to a ~9 times enhancement, i.e. ~9 times increase in the initial assay kinetics and (2) a ~7 times enhancement in the end values after 30 minutes.

Conclusion

We are able to generate strong flows of fluid and particles (~0.9 mm/s) near the surfaces of a closed fluid cell utilizing magnetic particles that are actuated by rotating magnetic fields. The magnetic particles assemble into microstirrers at the bottom cell floor in the presence of a vertical rotating magnetic field. By increasing the local fluid stirring by the individually rotating microstirrers, a global and strong vortex flow is generated and a cloud of particles is formed that translates along the upper and lower surface of the fluid cell. This phenomenon can produce significant and chaotic motion of microfluidic flows, which is important in achieving fast mixing and fast homogenization of biochemical reactions in microfluidic systems. For practical reasons we used a relatively low magnetic field strength of 30 mT, and the performance of the system could even be improved by using a stronger magnetic field since the micro-stirrers would be able to follow the rotating field without breaking at higher rotation frequencies, creating stronger global flow. Specifically, we observed a total re-suspension of fluorescent tracer-particles which were initially sedimented on the bottom surface of the fluid cell, by turning the rotating vertical field on for 1 min, indicating the capacity of fast mixing/homogenization of fluids. Moreover, we utilized the collective particle motion to enhance biochemical assays with magnetic capture particles and IgG assay targets. When compared to reference measurements (no external fields), magnetic actuation leads to both a ~9 times increase of the initial assay kinetics as well as a ~7 times increase of the end signals after 30 minutes.

Acknowledgements

This work forms part of the research programme of the Technology Foundation STW, STW project 10458.

Notes and references

[a] *Department of Mechanical Engineering, Eindhoven University of Technology, Den Dolech 2, 5600 MB Eindhoven, the Netherlands. E-mail: J.M.J.d.Toonder@tue.nl*
[b] *Institute for Complex Molecular Systems (ICMS), Eindhoven University of Technology, P.O. Box 513, 5600 MB Eindhoven, The Netherlands*
[c] *Department of Applied Physics, Eindhoven University of Technology, Den Dolech 2, 5600 MB Eindhoven, the Netherlands*

† Electronic Supplementary Information (ESI) available: [Movies S1-S7, Time-dependent formation of collective motion, Triaxial control, Biochemical assay protocol]. See DOI: 10.1039/b000000x/

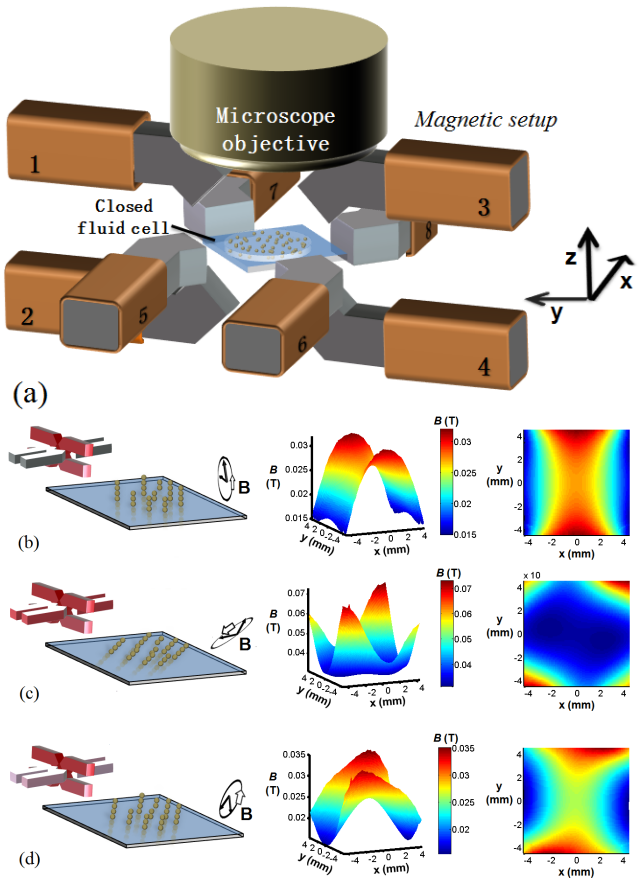

Fig.1 (a) Schematics of the eight-pole electromagnetic setup, and computed magnetic field distributions for various magnetic actuation configurations. (b) A vertical rotating magnetic field is applied using the vertical poles 1-4 (red) and the magnetic particles form rotating chains orthogonal to the fluid cell surface. We plot the corresponding time-averaged magnitude of the magnetic field over one rotational cycle over the entire cell region at z=0, i.e. the fluid cell floor, obtained by computer simulations. A narrow band region (between x=-2 mm and x=2 mm) with high field strength is seen to exist. (c) The combination of a horizontal and a vertical rotating magnetic field with equal magnitudes and equal frequencies. Isolated islands of dominant field strengths appear which are located near the horizontal poles (5-8). (d) The vertical magnetic field magnitude is 4 times larger than the horizontal field magnitude and the band region of high field strengths is restored.

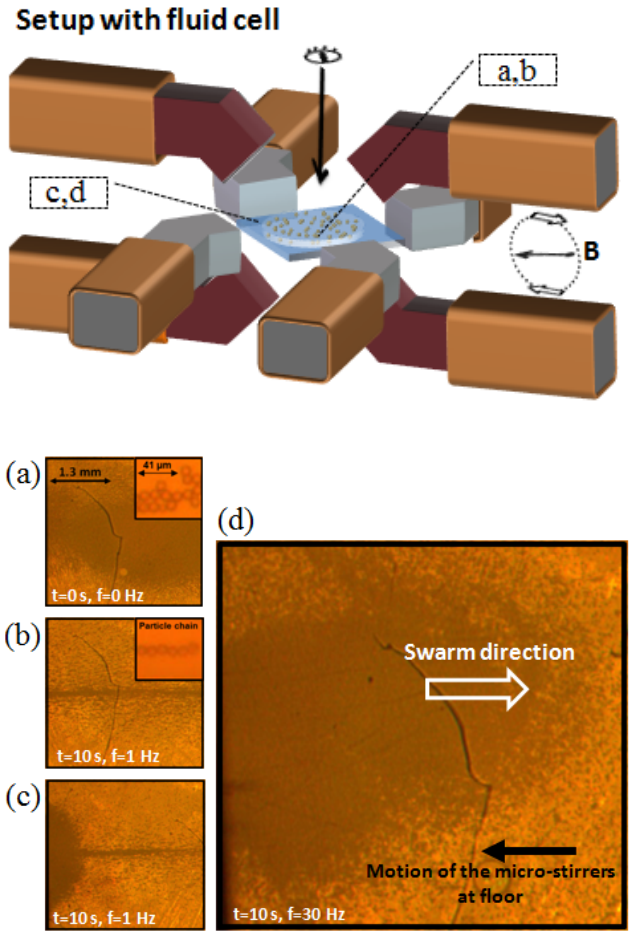

Fig.2 Images of magnetic microparticles within the fluid cell as a function of various actuation scheme. The fluid cell is a flat cylindrical chamber with a diameter of 9 mm and height of 600 µm. The location of the images shown in (a)-(d) are indicated in the schematic of the setup depicted on the top. (a) No field is applied and a suspension of magnetic particles is seen at cell floor. (b) and (c) A clockwise rotating vertical magnetic field (B, 30 mT, 1 Hz) is applied and due to field gradients, the formed particle chains are concentrated near the center and at the opposite ends of the fluid cell, terminating the translational and rotational movements of the microstirrers. (d) At a rotational frequency of 30 Hz, the magnetic gradient forces are overcome and a chaotic backflow of particles at the upper surface of the fluid cell is observed. Movies of the experiments can be found at Video S1, S2 and S3 in the Electronic Supplementary Information.

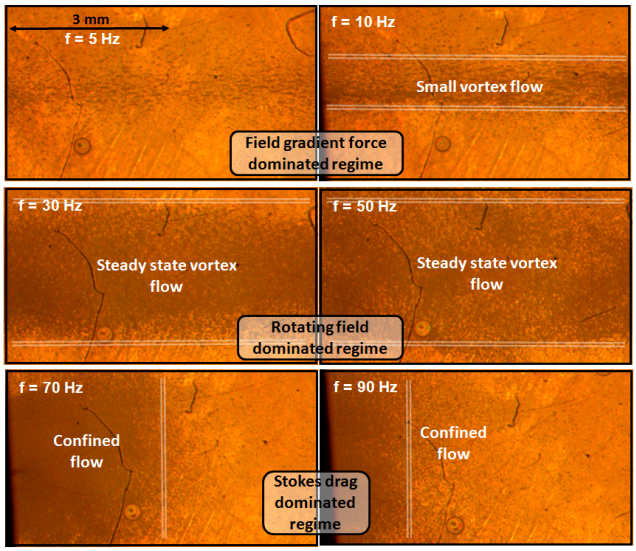

Fig. 3: The different regimes of swarming particles. A clockwise rotating vertical magnetic field (30 mT) is applied and we observe the final shape of swarming particles at different rotational frequencies of the applied field. A steady state vortex flow that is not diminishing over time and that is stretched along the entire length of the fluid cell, is found to exists between 30 and 50 Hz. Movies of the experiments can be found at Video S4 in the Electronic Supplementary Information.

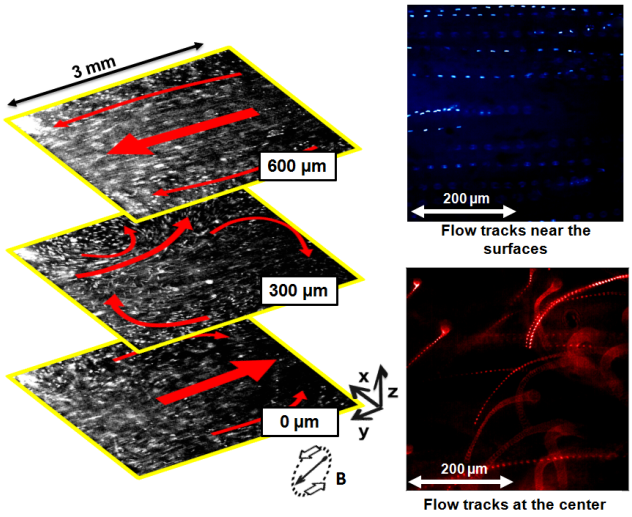

Fig. 4: Qualitative analysis of the flow field induced by a steady counter-clockwise rotating vortex flow of magnetic particle chains (rotating magnetic field of 30 mT, 30 Hz). The global induced motion (red arrows) of the fluorescent tracer particles (white spots) is indicated in three planes over the height of the cell. A global counter-clockwise rotating fluid vortex is observed. Near the bottom (z=0 µm) and upper (z=600 µm) surfaces of the fluid cell, the flow field is unidirectional. At the center of the cell (z=300 µm), small and local vortices appear. At the right-side of the figure: the corresponding tracks of the tracer particles were captured by superimposing 20 and 50 frames at 30 frames a second. Movies of the experiments can be found in Video S6 in the Electronic Supplementary Information.

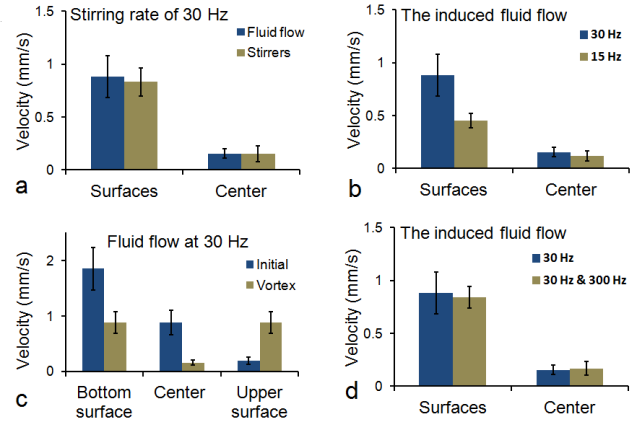

Fig. 5: Quantitative measurements of the induced flow. (a) A vertical rotating magnetic field (30 Hz) is applied and we obtain the absolute translational velocities of both the tracer particles and the magnetic particle chains within different horizontal planes in the fluid cell. (b) A two-fold lower stirring rate of the magnetic particle chains (15 Hz) causes the global induced fluid flow near the surfaces to halve (~0.45 mm/s). (c) In the initial stage (within 3 s after actuation), all the magnetic particles are present on the bottom surface and a maximum fluid flow is generated. At the final (vortex) stage (after 4 min of actuation), the distribution of the particles is divided between the two surfaces which causes the induced flow at the bottom surface to halve, and to increase at the upper surface. (d) A single rotating vertical field (30 mT, 30 Hz) is compared with a combination of vertical (30 mT, 30 Hz) and horizontal (5 mT, 300Hz) magnetic fields in the final vortex stage.

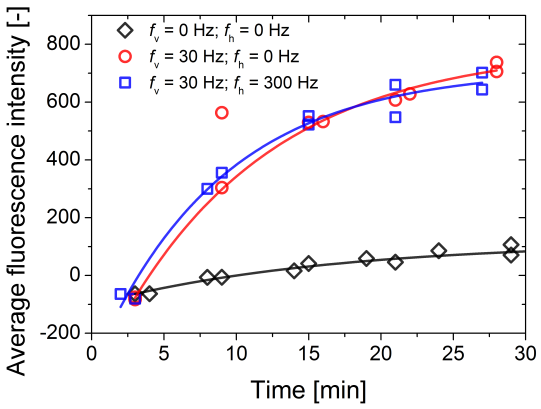

Fig 6: Results obtained from biochemical assay experiments where magnetic particles (~4000 µL) coated with Protein G proteins were actively agitated to capture the dispersed IgG (500 pM) assay targets marked with fluorescent labels. The amount of captured targets is indicated by the net fluorescence intensity (y-axis) emitted from the magnetic particles, averaged over 10^3 magnetic capture particles. Three sets of experiments were conducted: (black diamond) passive/reference measurements with no external fields, (red circle) A single vertical rotating magnetic field (30 mT, 30 Hz) and (blue square) a combination of vertical (30 mT, 30 Hz) and horizontal (5 mT, 300 Hz) rotating magnetic fields. The application of the fields leads to strong and global vortical flows of fluid and particles. The data are fitted using the following function: $y = A + B(1 - e^{-kt})$ where Bk is the initial slope of the target capture signals.

References

1 M. Vilfan, A. Potocnik, B. Kavcic, N. Osterman, I. Poberaj, A. Vilfan, and D. Babic, Self-assembled artificial cilia, *Proc. of Nat. Acad. Sci.,* 2010, **107**, 1844–1847.
2 C. E. Sing, L. Schmid, M. F. Schneider, T. Franke, and A. Alexander-Katz, *Proc. of Nat. Acad. Sci*., 2010, **107**, 535–540.
3 J. E. Martin, L. SheaRohwer, and K. J. Solis, Strong intrinsic mixing in vortex magnetic fields, *Phys. Rev. E.*, 2009, **80**, pp. 016312.
4 S. L. Biswal, and A. P. Gast, *Anal. Chem.,* 2004, **76**, 6448–6433.
5 T. Franke, L. Schmid, D. A. Weitz, and A. Wixforth, *Lab Chip*, 2009, **9**, 2831–2835.
6 T. Roy, A. Sinha, S. Chakraborty, R. Ganguly, and I. K. Puri, Magnetic microsphere-based mixers for microdroplets, Physics of Fluids, 21 (2009), pp.027101.
7 S. H. Lee, D. v. Noort, J. Y. Lee, B. Zhang, and T. H. Park, *Lab Chip*, 2009, **9**, 479–482.
8 J. T. Lee, A. Abid, K. H. Cheung, L. Sudheendra, and I. M. Kennedy, *Microfluid Nanofluid*, 2012, **13**, 461–468.
9 K. Tanaka, and H. Imagawa, *Talanta*, 2005, **68**, 437–441.
10 Y. Moser, T. Lehnert, and M. A. M. Gijs, Lab Chip, 2009, **9**, 3261–3267.
11 A. Ranzoni, J. J. Schleipen, L. J. van IJzendoorn, and M. W. J. Prins, *Nano. Lett*., 2011, **11**, 2017–2022.
12 A. van Reenen, A. M. de Jong, and M. W. J. Prins, *J. Phys. Chem. B*, 2013, **117**, 1210–1218.
13 A. van Reenen, A. M. de Jong, J. M. J. den Toonder, and M. W. J. Prins, *Lab Chip*, 2014, **14**, 1966-1986.
14 N. Pamme, *Lab Chip*, 2006, **6**, 24-38.
15 M.A.M. Gijs, *Microfluid Nanofluid*, 2004, **1**, 22-40.
16 T. G. Kang, M. A. Hulsen, P. D. Anderson, J. M. J. den Toonder, and H. E. H. Meijer, *Phys. Rev. E*., 2007, **76**, 066303.
17 Y. Gao, A. van Reenen, M. A. Hulsen, A. M. de Jong, M. W. J. Prins, and J. M. J. den Toonder, *Microfluid Nanofluid*, 2014, **16**, 265–274.
18 A. van Reenen, Y. Gao, A. M. de Jong, M. A. Hulsen, J. M. J. den Toonder, and M. W. J. Prins, *Proceedings of the 3rd European Conference on Microfluidics*, 2012, pp. 41.
19 Y. Gao, M.A. Hulsen, T.G. Kang,and J. M. J. den Toonder, *Pys. Rev. E,* 2013, **86**, 041503.
20 S. H. Behrens, and D. G. Grier, *J. Chem. Phys*., 2001, **115**, 6716.
21 A. Bricard, J. B. Caussin, N. Desreumaux, O. Dauchot, and D. Bartolo, *Nature*, 2013, **503**, 95–98.
22 T. Vicsek, A. Czirok, E. BenJacob, I. Cohen, and O. Shochet, *Phys. Rev. Lett*., 1995, **75**, 12261229.
23 J. Toner, Y. Tu, and S. Ramaswamy, *Ann. Phys*., 2005, **318**, 170244.
24 C. M. Marchetti, Hydrodynamics of soft active matter, *Rev. Mod. Phys.*, 2013, **85**, 11431189.
25 T. Vicsek, and A. Zafeiris, *Phys. Rep*., 2012, **517**, 71140.
26 S. Melle, O. G. Calderon, M. A. Rubio, and G. G. Fuller, *Phys. Rev. E*., 2003, **68**, 041503.
27 Y. Chena, J. Caia, Q. Xua, and Z. W. Chen, *Mol Immunol*., 2004, **41**, 1247–1252.